A dynamical Interpretation of Sequential Decay in Reactive Scattering

Francisco Gonzalez Montoya[1,2], Christof Jung[3], and Thomas H Seligman[3]

[1] School of Chemistry, University of Leeds, Leeds, LS2 9JT, United Kingdom.
[2]Centro Internacional de Ciencias AC - UNAM, Avenida Universidad 1001, UAEM, 62210 Cuernavaca, Morelos, México.
[3]Instituto de Ciencias Físicas, Universidad Nacional Autónoma de México, Av. Universidad s/n, 62251 Cuernavaca, México

April 14, 2023

Abstract

The topic of this article is a dynamical explanation of the sequential decay in rearrangement scattering. The essential observation is the behaviour of trajectories close to the basin boundary of the breakup channel. As a most simplistic example of demonstration, we use a version of the perturbed three particle Calogero–Moser system in a 1-dimensional position space.

1   Introduction

In reactive scattering, the following possibility has been well known for a long time. A projectile collides with a compound target resulting in some fragment leaving the interaction region immediately and a remaining compound fragment which decays after some time, which can be large compared to the first stage of the reaction. In the end, we have three or even more fragments in the final asymptotic state of the scattering event. Such multistep processes are known under the name sequential decay. In the present article, we relate these events to some newer developments in dynamical system theory in general and chaotic scattering in particular. More specifically, the purpose is to relate the phenomenon of sequential decay to the properties of the basin boundaries of the various arrangement channels of the system. This will lead in the end to a dynamical explanation.

The motivation of this study was in part the importance of sequential decay in nuclear physics, which has its origin in the decay chains of radioactive elements. In the analysis of nuclear reaction data and molecular breakup sequential decay is a frequent phenomenon. Goldansky's 1960 paper on double proton decay [1] is an instructive example of such work, while [2] would be an early reference for sequential decay in molecular physics. Note that the sequential decay in the nuclear three body problem is not very relevant due to the absence of resonances in these systems. Yet recent experiments with Boromean halo states, which we discuss below, appear with a strong di-neutron signature.

It turns out that in many nuclear reactions on light nuclei a clear separation of direct reactions and compound reactions can be made and in these cases, the decay of the compound nucleus usually can be described as sequential. In heavier nuclei precompound reactions can perturb the picture, but it still largely holds. In nuclear fission, the case of spallation obviously is an example where decay is not sequential, and in high energy reactions, we may see explosions of the nucleus. Nevertheless, sequential decays will occur frequently even where they are not dominant. The corresponding literature is vast with a recent surge of interest in Hoyle states and related alpha particle models for alpha like nuclei [3, 4, 5, 6, 7, 8, 9, 10, 11]. Recent experiments go beyond this in the sense that Borromean halo states open a new field where sequential decay products can be relevant [12, 13]

The sequential breakup of molecules has recently attracted much attention as the excitation with femtosecond laser pulses has become feasible. The dissociation of CO_2 may be the nearest we have to our toy model, though there is still a significant difference in the fact that the model has its three particles in one dimension rather than in three [14, 15].

Now the purpose of the present article is to give a dynamical explanation of sequential decay with the help of an appropriate model system in the similar spirit that other reaction dynamics in chemistry have been explained with the help of classical models, see for example [16, 17]. To keep all explanations on a level as simple as possible we try to construct the most minimalistic model system which shows sequential decay. As has become clear from the initial paragraph of this introduction we need at least 3 particles to have the possibility of a final arrangement channel with 3 fragments. To keep the configuration space as simple as possible, we study a 3 particle model in a 1-dimensional position space, i.e. we look at collinear scattering. After a separation of the centre of mass motion, the total system is reduced to a 2 degrees of freedom system, where all important structures in the configuration space and also most explanations in the phase space can be illustrated by 2-dimensional plots.

For the 2 particle interaction potentials between the various pairs of particles we take inverse squares of hyperbolic functions of position coordinates. These potential functions have the great advantage that most quantities in the asymptotic dynamics can be expressed in closed form by elementary functions. This holds in particular for the transformation to action and angle variables for the internal dynamics of 2 particle fragments. The model is constructed and explained in all the details in section 2.

It will turn out that sequential decay occurs for a small layer of initial conditions belonging to the basin of the 3 fragment break up channel and lying close to the basin boundary of the break up channel. Accordingly in section 3 we will concentrate on the basin boundaries and the trajectories running close to these basin boundaries. Frequently we apply procedures which have been developed before in a previous investigation of the break up channel, see [18]. Section 4 gives conclusions and some final remarks.

2 Perturbed Calogero-Moser system

2.1 The perturbed three particle Calogero-Moser system with hyperbolic potentials

As an example of demonstration, we use the version of the perturbed Calogero-Moser system with hyperbolic 2-particle potentials. See references [19, 20] for more details about the properties of the model and its phase space analysis. Let us assume 3 particles called A, B, and C moving along a 1-dimensional position space, i.e. we study collinear scattering. The masses of the particles are equal to 1 and the position coordinates of the particles are q_A, q_B and q_C respectively. The conjugate momenta are p_A, p_B and p_C respectively. We assume that the particle pair A and B, and also the particle pair B and C have an attractive 2-particle interaction, whereas the particle pair A and C has a repulsive 2-particle interaction.

For the total Hamiltonian we take the model system

$$H = \frac{1}{2}(p_A^2 + p_B^2 + p_C^2) - \frac{D_A}{\cosh^2(q_B - q_C)} + \frac{D_B}{\sinh^2(q_C - q_A)} - \frac{D_C}{\cosh^2(q_A - q_B)}. \tag{1}$$

We choose D_B as the unit of energy and thereby D_B takes the numerical value 1. Next, we assume that the particles A and C are equal and therefore D_A and D_C have the same numerical value D. That is, we will study the case $D_B = 1 \neq D_A = D_C = D$ in the following, where only positive values of D make sense.

The figures 1, 2, 3 show examples of the scattering process where the positions of the three particles (horizontal axis) are plotted as a function of time (vertical axis). The particles A, B, and C are represented by the blue, red, and green curve respectively. In Fig. 1 the three particles enter as free particles and in the long run also leave as free particles. In Fig. 2 the free particle A hits a bound state of the particles B and C and a reaction occurs where in the end the free particle C moves away from a bound state of the particles A and B. In Fig. 3 the free particle C hits a bound state of the particles A and B. This time the final state of the reaction are three free particles.
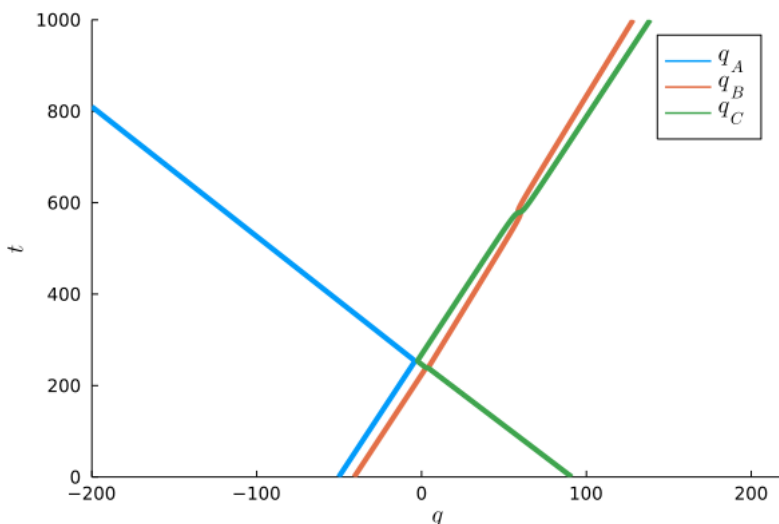

Figure 1: Position of the three particles vs time. The system starts with three free particles in the incoming asymptotic region, then the particles interact close to $q = 0$ and the system finishes again as three free particles. The potential is the perturbed Callogero-Moser potential from Eq. 1 for the nonintegrable case with $D_B = 1$, $D_A = D_C = 0.9$. We have the total energy $E=0.1$. The numerical calculation is done using the Taylor integrator order 25 implemented in [21] to keep the error in the energy small in all the trajectories, particularly when the particles are close and the standard numerical methods fail.
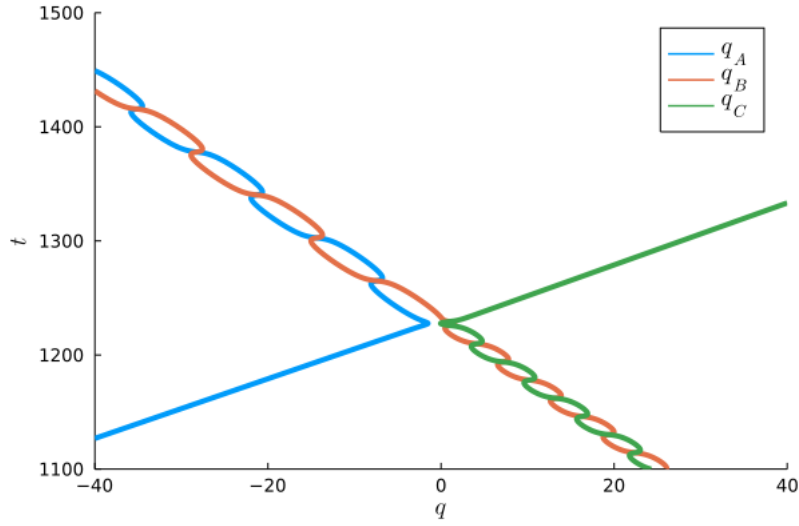
Figure 2: Position of the three particles vs time. The system starts as the free particle A and a bound state of the particles C and B and ends as a free particle C and a bound state of the particles A and B. The potential parameters have the same values as in Fig. 1 .
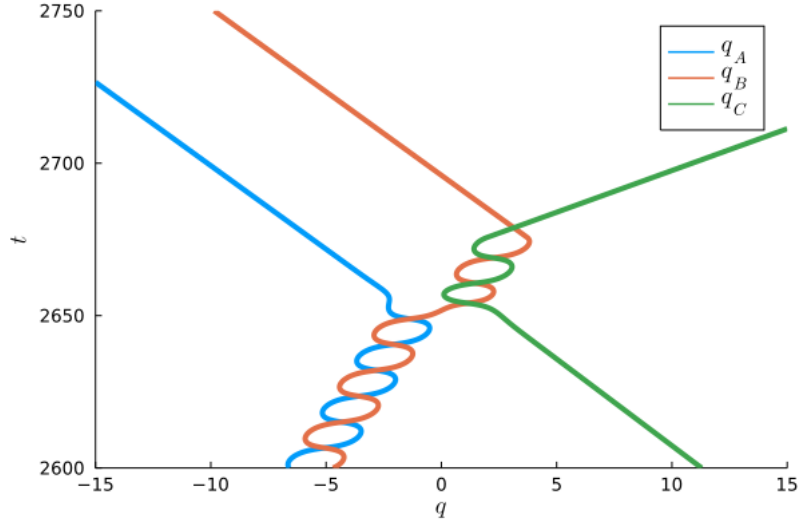

Figure 3: Position of the three particles vs time. The system starts again as a free particle C and a bound state of the particles A and B. However this time it ends as three free particles. The parameter values of the potential are the same as in Fig. 1.

In order to get rid of the centre of mass motion we transform to the centre of mass coordinate S and the relative coordinates R and r defined as

$$
\begin{aligned}
S &= (q_A + q_B + q_C)/3, \\
R &= \sqrt{1/6}(q_A + q_C - 2q_B), \\
r &= \sqrt{1/2}(q_C - q_A)
\end{aligned}
$$

(2)

and the corresponding conjugate momenta

3

$$
\begin{aligned}
p_S &= p_A + p_B + p_C, \\
p_R &= \sqrt{1/6}(p_A + p_C - 2p_B), \\
p_r &= \sqrt{1/2}(p_C - p_A).
\end{aligned}
\tag{3}
$$

From now on we do no longer care about the centre of mass degree of freedom (dof) and set S and P_S permanently to the value 0. In the new coordinates the Hamiltonian for the two relative degrees of freedom has the form

$$
H = \frac{p_R^2}{2} + \frac{p_r^2}{2} + V(R, r),
\tag{4}
$$

where the potential energy $V(R, r)$ is defined as

$$
V(R, r) = -\frac{D}{\cosh^2\left(\sqrt{3/2}R + \sqrt{1/2}r\right)} + \frac{1}{\sinh^2\left(\sqrt{2}r\right)} - \frac{D}{\cosh^2\left(\sqrt{3/2}R - \sqrt{1/2}r\right)}.
$$

Up to an unusual front factor, the new coordinates are the Jacobi coordinates as seen from the particle B. The front factors have been included in order to transform the reduced masses to the value 1. Remember that the transformation $p \to \sqrt{m}p$, $q \to q/\sqrt{m}$ is a canonical transformation.

A plot of the total potential is given in Fig. 4. Between the particles A and C we have a repulsion which becomes infinite for q_A approaching q_C. Therefore we can restrict all further considerations to the case that particle C is to the right of particle A, i.e. we can restrict the investigation to the half plane $r > 0$ of the configuration space of the relative coordinates. The total potential shows a curved valley whose bottom line converges to the straight line L_C given by $r = \sqrt{3}R$ for $R \to +\infty$ and to the straight line L_A given by $r = -\sqrt{3}R$ for $R \to -\infty$.

Far away from these two straight lines and also far away from the r axis the potential goes to zero exponentially fast. In Fig. 4 we can appreciate well how the potential converges to straight potential channels for large values of the coordinate r. In the central region where all three potential contributions are important, we see how the potential valley makes a curve in this interaction region.
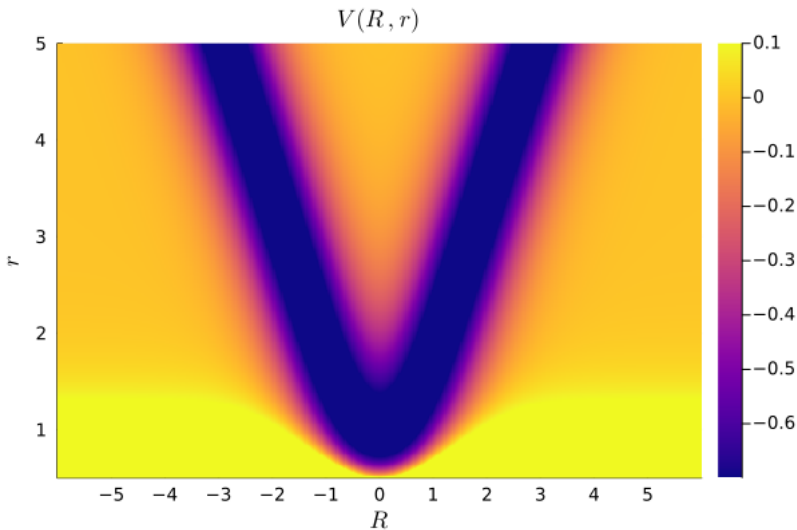

Figure 4: Potential energy $V(R, r)$ in colour scale as a function of the relative coordinates R and r. The values of the parameters are $D_B = 1$, $D_A = D_C = 0.9$. The potential energy surface has a valley plotted in dark colour. In the asymptotic region, the branch of the valley on the right corresponds to the scattering channel C and the other branch on the left to the channel A. The potential energy goes to infinity on the line $r=0$ and is almost flat outside the valley and for r large.

The simplest and shortest periodic orbits always play an important role in the dynamics. In our case, it is clear by symmetry arguments that for a negative value of the total energy there exists a simple periodic orbit γ oscillating along the r axis in the potential valley.

The bottom line of the potential valley has a 1:1 projection on the R axis and later we call v the coordinate along the potential valley where between v and R a 1:1 relation holds. That is, v is the reaction coordinate along the valley. We call u the coordinate perpendicular to v and pointing in the positive r direction.

The part of the valley for R large and positive will be called the potential channel C. And the part of the valley for R large and negative will be called the potential channel A.

Fig. 5 gives the 3 trajectories shown before in Figs. 1, 2, 3 again but this time plotted as curves in the space of the relative coordinates. The blue curve is the trajectory from Fig. 1, the green curve is the trajectory from Fig. 2 and the orange curve is the trajectory from Fig. 3.
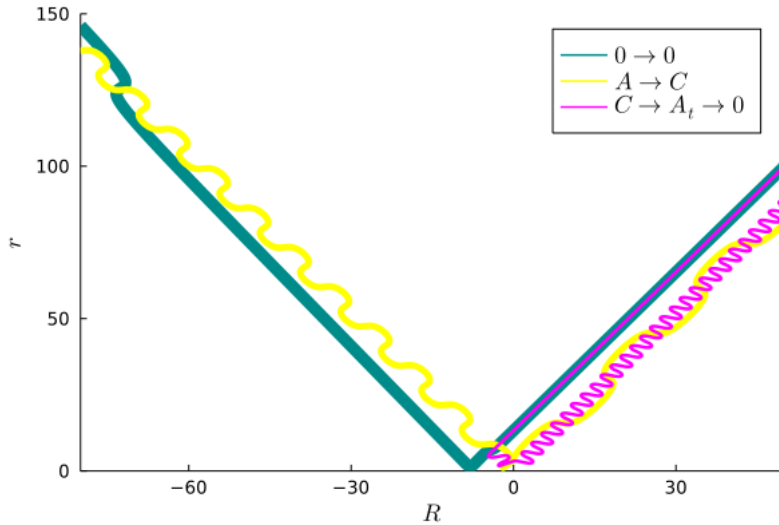

Figure 5: The trajectories plotted in relative coordinates R and r which have already been shown before in 3 particle coordinates in Figs. 1,2,3. We can appreciate how the potential energy in Fig. 4 defines the scattering channels. The trajectory that goes from channel C to channel 0, corresponding to Fig. 3, has a transient behaviour close to the origin. This transient motion is represented by the segment of the trajectory with $R < 0$.

2.2 The asymptotic arrangement channels and their asymptotic labels

In a system consisting of 3 particles we have various possibilities to group these particles into fragments and form bound states. First, for $D > 1$ and for a total energy E smaller than the asymptotic depth $-D$ of the potential valley, i.e. for $E < -D < -1$, only 3 particle bound states exit. They are not relevant for the topic of the present article. Second, there is the possibility of a bound state of the particles B and C bound together and the particle A moving freely and far away from B and C. Such states will be called states in the arrangement channel A and their trajectories move in the channel A of the potential. Next, there are states where the particles A and B are bound together and the particle C moves freely and far away from the particles A and B. Such states are called arrangement C and their corresponding trajectories move in the channel C of the potential. In our particular model, the particles A and C have a repulsive interaction. Therefore an arrangement B does not exist, where particle B would move freely relative to a bound state of the particles A and C. Finally, there exists the breakup channel, also called arrangement channel 0, where all 3 particles move freely and asymptotically any particle moves far away from the other particles. They correspond to trajectories in the position space of relative coordinates far away from the potential valley and also far away from the R axis, i.e. in the region where the tails of all potentials are exponentially small.

First, let us look at the case $D > 1$ where there exists on the r axis a local minimum of the total potential with energy $E_m < -D$ and we have only 3 particle bound states in the energy interval $(E_m, -D)$. For total energies E in the interval $(-D, 0)$ the trajectories belonging to the chaotic invariant set form 3 particle bound states. Trajectories running along the stable manifolds of localized subsets can start in the initial arrangement A or C and they end as 3 particle bound states. However, such trajectories only occupy a subset of measure 0 in the energy shell. Trajectories running on unstable manifolds of localized subsets show the corresponding time reversed behaviour. Stable 3 particle bound states can exist in KAM islands around stable periodic orbits. The rest of the phase space is occupied by trajectories leaving along the potential valley in the past and also in the future.

For $D < 1$ there is a saddle point of the potential along the r axis with saddle energy $E_s > -D$ and the periodic orbit γ is the only 3 particle bound state. For an energy in the interval $(-D, E_s)$ trajectories starting in channel A return to channel A and trajectories starting in channel C return to channel C. For energies in the interval $(E_s, 0)$ transitions from channel A to channel C and vice versa become possible. Here trajectories running on the unstable or the stable manifolds of the periodic orbit γ are exceptions of measure 0 which start or end as 3 particle bound states respectively.

For energies $E > 0$ also the channel 0 is energetically accessible. That is, for a positive total energy trajectories starting in the channels A or C can end in channel 0 by breakup processes. For very well selected initial conditions also

the reverse can happen, i.e. trajectories starting in the channel 0 can end in one of the 2-fragment channels. However, such processes need a very delicate preparation of the initial conditions and are of little practical importance. Some of these possibilities have already been illustrated by the Figs. 1, 2, 3, 5.

For our particular case of study there are no localized orbits for positive energies and therefore also no stable or unstable manifolds of localized subsets. As a consequence for $E > 0$ we also do not have trajectories which start or end as 3-particle bound states.

To describe the motion in the asymptotic channels A and C we use the coordinates u and v already mentioned before. They are defined in terms of the coordinates R and r in the channel A as

$$
\begin{aligned}
u &= \sqrt{3}R/2 + r/2, \\
v &= R/2 - \sqrt{3}r/2
\end{aligned}
\tag{5}
$$

and in channel C as

$$
\begin{aligned}
u &= -\sqrt{3}R/2 + r/2, \\
v &= R/2 + \sqrt{3}r/2.
\end{aligned}
\tag{6}
$$

Asymptotically in the channels A and C the motions in longitudinal and in transversal direction separate. The asymptotic Hamiltonian has in both cases the functional form

$$
H_{as} = \frac{p_v^2}{2} + H_\perp(u, p_u),
\tag{7}
$$

where

$$
H_\perp(u, p_u) = \frac{p_u^2}{2} - \frac{D}{\cosh^2\left(\sqrt{2}u\right)}.
\tag{8}
$$

For negative values of the transverse energy, i.e. negative values of the Hamiltonian from Eq.8, it is convenient to transform the transverse motion (the u degree of freedom) to action and angle variables I, ϕ. For the $cosh^{-2}$ potential this transformation is well known in terms of elementary functions and here we only give the result

$$
I(u, p_u) = \sqrt{D} - \sqrt{-E_\perp},
\tag{9}
$$

$$
\phi(u, p_u) = \arcsin[\sqrt{-E_\perp/(E_\perp + D)} \sinh(\sqrt{2}u)],
\tag{10}
$$

where in Eqs. 9 and 10 for $E_\perp$ the Hamiltonian from Eq.8 has to be inserted. Inversion of Eq.9 gives

$$
H_\perp(I, \phi) = -(I - \sqrt{D})^2.
\tag{11}
$$

Note that the transformation to action and angle variables only makes sense when $E_\perp$, the energy in the transverse u degree of freedom is smaller than 0. As it must be for a 1-dof system, $H_\perp$ is independent of the angle and accordingly I is an asymptotically conserved quantity. The velocity ω of the angle ϕ is given as

$$
\omega = \frac{\partial H_\perp(I, \phi)}{\partial I} = -2(I - \sqrt{D}).
\tag{12}
$$

Next, we have to decide how we label asymptotes in the channels A and C. As in any Hamiltonian system we have as a first label the value of the total energy E. Second, we have the distribution of the energy between the longitudinal degree of freedom v and the transversal degree of freedom u. This can be done by giving either the value of the longitudinal momentum p_v (equivalent to giving the longitudinal kinetic energy) or equivalently by giving the transversal action I (equivalent to the transversal energy). Finally, we need a quantity which gives the relative phase shift between the longitudinal and the transversal motion. This is a reduced angle variable which is constant in the asymptotic region. We can use the reduced angle variable ϕ_{red} defined as

$$
\phi_{red} = \phi - \omega \frac{v}{p_v}.
\tag{13}
$$

Note that the 3 asymptotic labels E, I and ϕ_{red} are constant along the asymptotic motion in the 2-fragment channels. Therefore they are appropriate to label initial or final asymptotes.

Of course, these label are not appropriate for asymptotes in channel 0. In the breakup channel asymptotic trajectories are straight lines whereas the first two labels we can use either the total energy and the direction of the momentum θ or equivalently the vector momentum. As a third label we use either the impact parameter relative to the origin or equivalently the angular momentum of the trajectory. Note that also these 3 asymptotic labels are constant along asymptotic trajectories of the channel 0. Thereby the asymptotic motion is superintegrable in any case and in any asymptotic channel.

2.3 Integrability properties

The 2 particle potentials all depend on differences between the particle coordinates only. Therefore the total momentum of the system p_S is a conserved quantity and we have already separated away the centre of mass motion by a transition to relative coordinates. As in all Hamiltonian systems, the Hamiltonian function is a second conserved quantity. And if all 3 potential strengths D_A, D_B and D_C have the same numerical value (which we can set to the value 1 in this case) then we even have a third conserved quantity K in closed form in terms of elementary functions.

$$K = p_A p_B p_C + \frac{p_A}{\cosh^2(q_B - q_C)} - \frac{p_B}{\sinh^2(q_A - q_C)} + \frac{p_C}{\cosh^2(q_A - q_B)}. \tag{14}$$

For a detailed discussion of this very particular case see [19].

If the 3 coupling parameters D_A, D_B, and D_C are not equal then the conserved quantity K does not exist any longer. In the case studied in this article, namely $D_B = 1$, $D_A = D_C = D$ the properties of chaos are as follows. For $D > 1$ and $-D < E < 0$ we find a chaotic invariant set in the phase space, a chaotic saddle. In a Poincaré map with the intersection condition $u = 0$ with a specific intersection orientation it is represented by a ternary symmetric horseshoe where the outer fixed points sit at $v = \pm\infty, p_v = 0$ and the central fixed point sits at $v = 0, p_v = 0$. In this chaotic case, general scattering trajectories show transient chaos and the scattering functions show a fractal set of singularities as it is usual for chaotic scattering. For general information on transient chaos and its relationship to chaotic scattering see [22] and chapter 6 of [23]. For publications on chaotic scattering with an explanation of many concepts which we will mention later briefly without any detailed explanation see also [24, 25] and chapter 4 in [26]. For the intriguing relation between the integrability of the Hamiltonian and the integrability of the S-matrix see [20].

For $D < 1$ the only localized trajectory for $E < 0$ is the periodic orbit γ oscillating along the r axis. Accordingly, there is no chaotic saddle and no scattering chaos. In this case, a third conserved quantity could be constructed by the transport of any asymptotic initial condition over the subset S of the phase space consisting of the complete phase space without points lying on γ or its stable and unstable manifolds. For example, to any point $x \in S$ we construct the trajectory through x and assign to x the value of I on the initial asymptote of this trajectory. This quantity is constant along any trajectory by construction and it defines a smooth function on the subset S. Note that in the presence of a chaotic saddle with its fractal geometry this procedure would not result in a piecewise smooth function on the phase space.

For $E > 0$ this construction also works for all points belonging to trajectories with an incoming asymptote in one of the 2 fragment channels. For points lying on trajectories with an initial asymptote in channel 0 we can use instead the initial direction of the momentum θ and assign it to all points along the trajectory. This procedure constructs a piecewise smooth function on the phase space. Note, that for $E > 0$ no localized trajectories exist. Therefore there is no need to take away periodic orbits and their stable and unstable manifolds from the domain of this construction. The only exceptional subset is the boundary of the basin of the channel 0 which will be studied in the next section.

3 Basin boundary of the breakup channel

We can divide all points x of the phase space into various subsets according to the channel in which the trajectory through this point x ends in the far future. The basins of the channels A, C, and 0 are all such initial points x whose trajectories end up in channel A, C or 0 respectively. These basins will be called B_A, B_C and B_0 respectively. Initial points lying on stable manifolds of localized subsets or on the localized subsets themselves do not end in any one of the asymptotic channels A, C or 0. Therefore they do not belong to any one of the basins B_A, B_C or B_0 respectively. We call this subset B_L.

Usually, the boundaries between the various basins are either stable manifolds of localized subsets or they are stable manifolds of particular subsets of final asymptotes. For a negative total energy E and $D > 1$ the phase space contains a chaotic saddle and its stable manifolds are the boundary between the channels A and C. For a chaotic saddle, its stable manifolds form a fractal and therefore also the basins and their boundaries are fractal.

For $D < 1$ and $E \in (-D, E_s)$ the basins of the channels A and C are well separated in the position space and do not have any common boundary, they are disjoint components of the energy shell. In this case, the basin boundaries consist of energetic boundaries only. For $D < 1$ and $E \in (E_s, 0)$ the energy shell has a single component only which is divided into B_A, B_C and B_L. The basin boundary is formed by the stable manifold of the periodic orbit γ.

For a positive total energy, the case studied in the present work, we do not have any localized trajectories. Therefore, there can not exist any stable manifolds of localized subsets of trajectories. This implies the absence of any chaotic saddle and of any fractal basin boundaries. In addition, there are no direct boundaries between B_A and B_C. When we deform a trajectory ending in channel A smoothly into a trajectory ending in channel C then the deformation process must pass through a set of trajectories ending in channel 0. Accordingly, the only boundaries which exist are boundaries between the basin B_A and B_0 and boundaries between the basins B_C and B_0. Because of the absence of chaos for positive E these boundaries can not be fractal. Compare the analogous arguments for the model system explained in [18]. Because of the discrete symmetry of the system, it is sufficient to study in the rest of this section trajectories starting in the channel A and to investigate in detail the boundary between the basins B_A or B_C and B_0.

3.1   Approach to the basin boundary from the side of the 2-fragment channels

In the next 2 subsections, we describe the behaviour of typical trajectories when their initial conditions approach the basin boundary. First we do it for the case when the initial condition approaches this boundary from the side of the 2 fragment channel A. If the trajectory ends in a 2 fragment channel then the final asymptote moves along the v coordinate with constant speed. Simultaneously it oscillates in the u direction with a frequency given by Eq. 12. The energy in the u degree of freedom ($E_\perp$ given by Eq. 11) is negative and approaches 0 from below when the initial condition approaches the basin boundary from the side of the 2 fragment channel. In the limit of the distance to the boundary going to zero the frequency from Eq. 12 also goes to zero, i.e. the oscillation period $T = 2\pi/\omega$ goes to infinity. If the trajectory moves in the v direction (i.e. along the axis of the potential channel from Fig. 1) with momentum p_v then the oscillation wavelength of the trajectory along the potential channel is $\lambda = p_v T$ and also goes to infinity when the initial condition (and therefore also the whole trajectory) approaches the basin boundary. In the limit of running exactly on the basin boundary, graphically at very large longitudinal distance v the trajectory seems to run parallel to the potential valley at a finite transverse distance.

It is common in scattering experiments that we prepare the total energy and also prepare the oscillation energy of the two particle fragments, in our case given by the oscillation action from Eq. 9. In contrast usually we do not have control over the reduced phase of the oscillation of the two particle fragment, in our case given by Eq. 13. We assume now that this reduced phase has a random distribution over the interval $[0, 2\pi]$. To study the trajectories close to the basin boundary we do the following. We fix in the incoming channel A values of $E = 0.01$ and $I = 0.91$, scan ϕ_{red} in the interval $[0, 2\pi]$ and let the trajectories run until they reach the outgoing asymptotic region.

For the very small energy $E = 0.01$ used from now on, we have in the whole domain $\phi_{red} \in [0, 2\pi]$ one interval where the trajectories end in channel A, one interval where the trajectories end in channel C, and in between two very short intervals where the trajectories end in channel 0.

Interesting for us is now the graphical presentation of the result in a region of ϕ_{red} which contains an interval ending in channel 0 and some small parts of the adjacent intervals ending in the 2 fragment channels. It is Fig. 6.

In part (a) of Fig. 6, the outgoing direction θ of the momentum is shown in the ϕ_{red} interval which leads to the final channel 0. Remember that this quantity θ only makes sense for the asymptotic channel 0. This angle has values between $\pi/3$ and $2\pi/3$. These limiting values are exactly the directions of the straight lines L_C and L_A respectively, i.e. the asymptotic directions of the potential valleys for the asymptotic channels C and A. This demonstrates graphically how the outgoing straight trajectory of the channel 0 becomes parallel to the asymptotic channel axis of the potential when the trajectory approaches the boundary of channel 0.

Part (b) of Fig. 6 shows the transverse energy of the outgoing asymptotes as function of the initial reduced phase ϕ_{red}. The blue curve gives the final asymptotic energy $E_{\perp,A}$ corresponding to the channel A and the yellow curve gives $E_{\perp,C}$ corresponding to the channel C . For the trajectories that ends in channel 0, we can use both definition of the transverse energy of the outgoing asymptotes to define $E_{\perp,0}$. A trajectory ends in channel A exactly when $E_{\perp,A} < 0$ and it ends in channel C exactly when $E_{\perp,C} < 0$. The boundary point between basins B_A and B_0 is the point where $E_{\perp,A} = 0$ and the boundary point between basins B_C and B_0 is the point where $E_{\perp,C} = 0$.
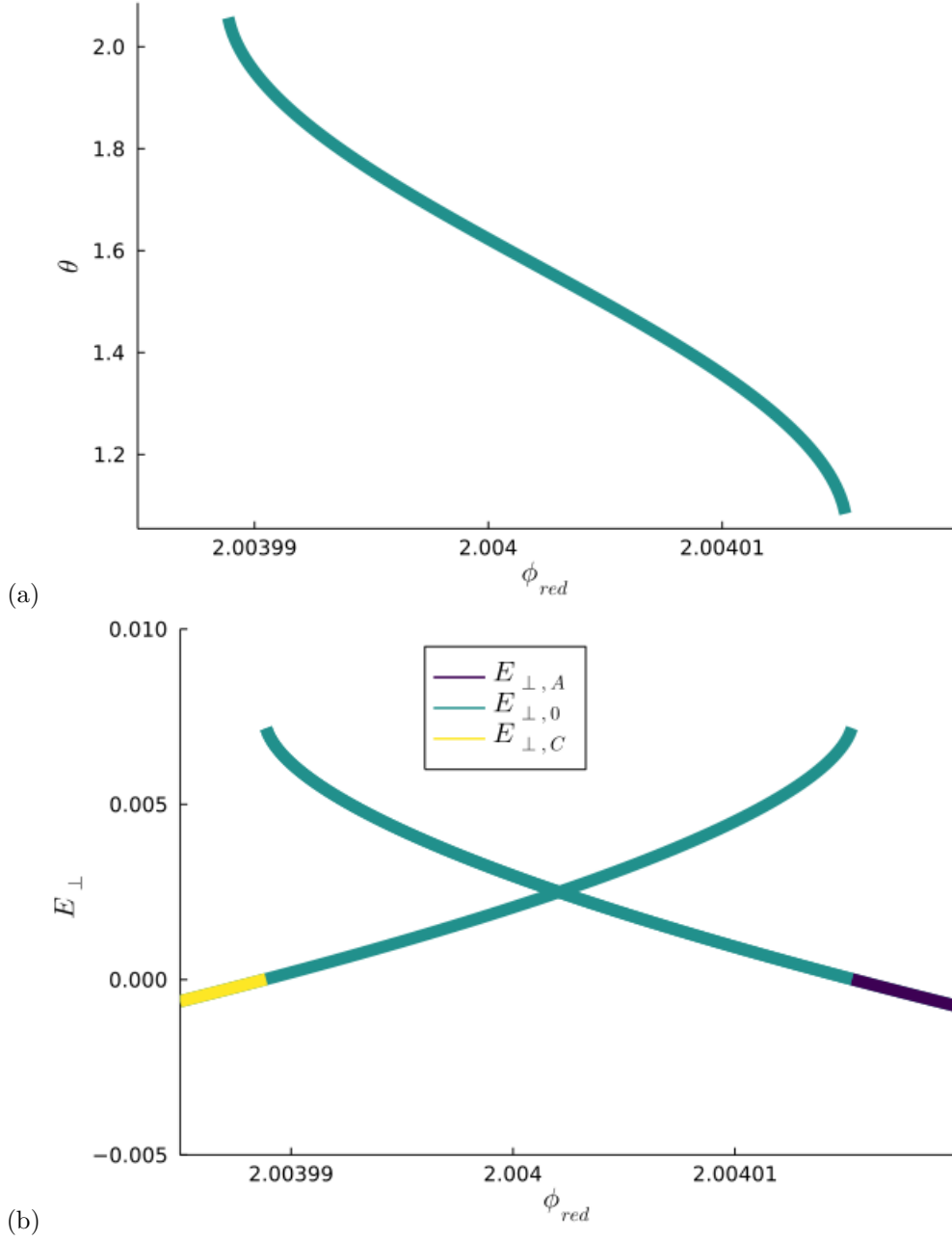
(a)

(b)

Figure 6: The final angle θ in the upper panel and the final transverse energies $E_{\perp,A}$ as the blue curve and $E_{\perp,C}$ as the yellow curve in the lower panel, all as a function of the initial reduced phase ϕ_{red}. For additional explanations see the main text.

In the next two figures, we show some trajectories in the position space running close to the basin boundary of channel 0. The Fig. 7 presents 6 trajectories close to the boundary between basins B_A and B_0 and Fig. 8 presents 6 trajectories close to the boundary between basins B_C and B_0. For each one of these figures there are three trajectories from the basin of the two fragment channel (panels (a), (b) and (c)) and three trajectories from the basin of the channel 0 (panels (d), (e) and (f)) respectively.

The panels (a), (b), (c) of Fig. 7 show a sequence of 3 trajectories in the position space where the initial condition comes closer to the basin boundary from the side of B_A. We observe how accordingly the oscillation period T in u direction and the wavelength λ along the v direction become larger. Eventually they converge to ∞ in the limit where the initial condition reaches the basin boundary. In the panels (a), (b) and (c) of Fig. 8 we see the corresponding behaviour when the initial condition approaches the boundary between B_C and B_0 from the side of B_C.

3.2 Approach to the basin boundary from the side of the breakup channel

Now let us look at trajectories where the initial condition lies close to the basin boundary but this time on the side of the 3 fragment channel 0. In this case, the energy in the u degree of freedom is small and positive. That is, the trajectory leaves the potential valley and in the long run the u coordinate becomes large positive or large negative. The relative angle between the asymptotic trajectory and the potential valley is slightly different from zero.

In the sequence of plots of trajectories in the position space in the panels (d), (e) and (f) of Fig. 7 the initial condition comes closer to the basin boundary between B_A and B_0 from the side of B_0. We observe how accordingly the asymptotically straight outgoing trajectory becomes more and more parallel to the channel axis of channel A. At the same time, the last crossing of the axis of the potential channel A is pushed out to larger values of the reaction coordinate v when the initial condition converges to the boundary point. In Fig. 8 the corresponding behaviour is illustrated near the boundary between B_C and B_0.

Importantly, very close to the boundary point it needs a very long observation time to distinguish such a trajectory ending in the channel 0 with very small positive transverse energy from one ending in the channel A with a negative transverse energy (here it is the bound state energy) very close to 0.

As a result, we have obtained the following dynamical picture of the phenomenon of sequential decay. If the initial conditions are close to the boundary of the basin B_0 with some two fragment channel X (where in our example of the perturbed Calogero-Moser system X can be either A or C) then in the collision the particle X separates rather quickly from the remaining set of particles with an energy clearly larger than 0. However, the remaining group of particles has a total energy a little larger than 0. Therefore this remaining group is close to be bound but not really bound and this remaining group dissolves slowly with very small kinetic energy between its fragments. Accordingly, it takes some time to observe clearly and without doubt the decay of this remaining group. The observer notices one particle (or fragment) leaving instantaneously and other particles (or fragments) separating later with very small relative kinetic energy, a typical sequential decay.

It depends on the observational resolution, where we make the distinction between sequential decay and direct decay into three or more fragments. On this somewhat arbitrary choice depends the width of the layer in basin B_0 along its boundary which leads to the observation of sequential decay. As a consequence also the relative fraction of scattering events which are classified as sequential decay depends on this choice when we shoot in a beam of fragments without any control over the reduced oscillation phase.

To give a pictorial impression of the basins for the various channels in the set of the initial conditions and also a partial picture of the basins in the phase space, one can do the following. We select an appropriate 2-dimensional plane in the set of all initial conditions, place a grid of many pixels on this plane and colour each one of this pixels according to which basin it belongs, i.e. according to the channel in which the corresponding trajectory ends in the far future.

In Fig. 9 we choose the ϕ_{red}–I plane for the fixed value of the total energy $E = 0.01$ and initial conditions in the channel A. Pixels whose corresponding trajectories end in channel C and coloured yellow. Pixels whose trajectories end in channel A are coloured cyan. And pixels whose trajectories end in channel 0 are coloured dark blue. In contrast in Fig. 10, we fix the transverse action I at the value 0.91 and choose the ϕ_{red}–E plane in the initial channel A and apply the same procedure as in the previous figure to colour the pixels. We observe that for these initial conditions most of the trajectories end in channel C, i.e. they just advance along the potential channel with a monotonically increasing reaction coordinate. Only for a small fraction of the initial condition the trajectory does something more complicated in the interaction region, interchanges strongly transversal and longitudinal energy and thereby manages to end in channel A or in channel 0.

Basically the domains of the plots are divided into layers belonging to the various final channels. Partially these layers are extremely thin, thinner than the pixel resolution. Therefore partially the stripes belonging to the various channels look broken into disjoint pieces, whereas in reality they should be continuous stripes going around in ϕ_{red} direction. This appearance of extremely thin layers seems to be a general phenomenon. It has also been observed in the Refs. [27, 28] in model calculations for molecular reactions. The corresponding layers in the complete phase space are obtained by the transport of these layers in the set of the asymptotic initial conditions by the flow.
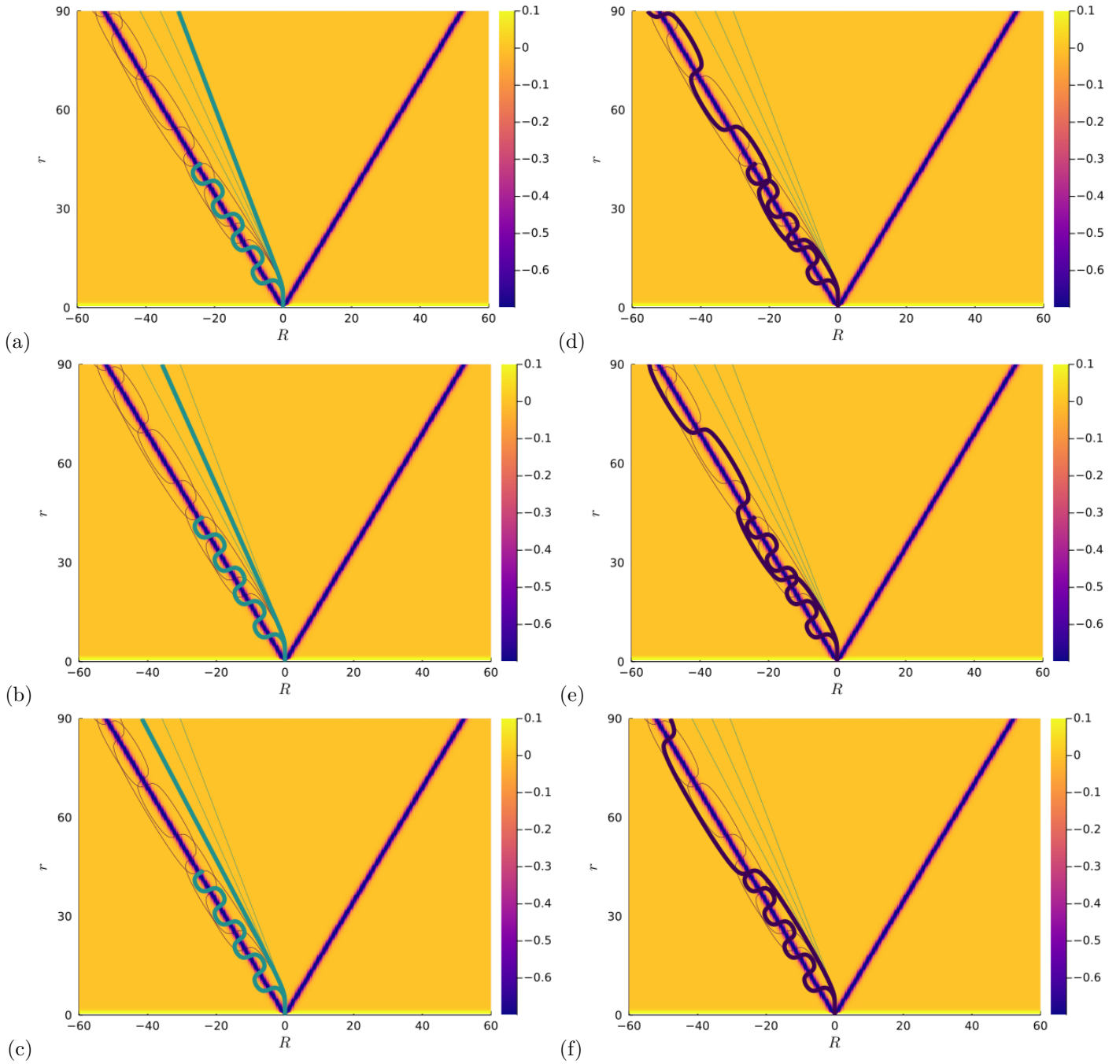
Figure 7: Trajectories close to the boundary between final asymptotic channels A and 0. $E = 0.01$, $D = 0.9$. The trajectories highlighted on the left panels end in the channel 0 and the trajectories highlighted on the right panels end in the channel A. The trajectories highlighted on lower panels are close to the boundary between channel A and 0.
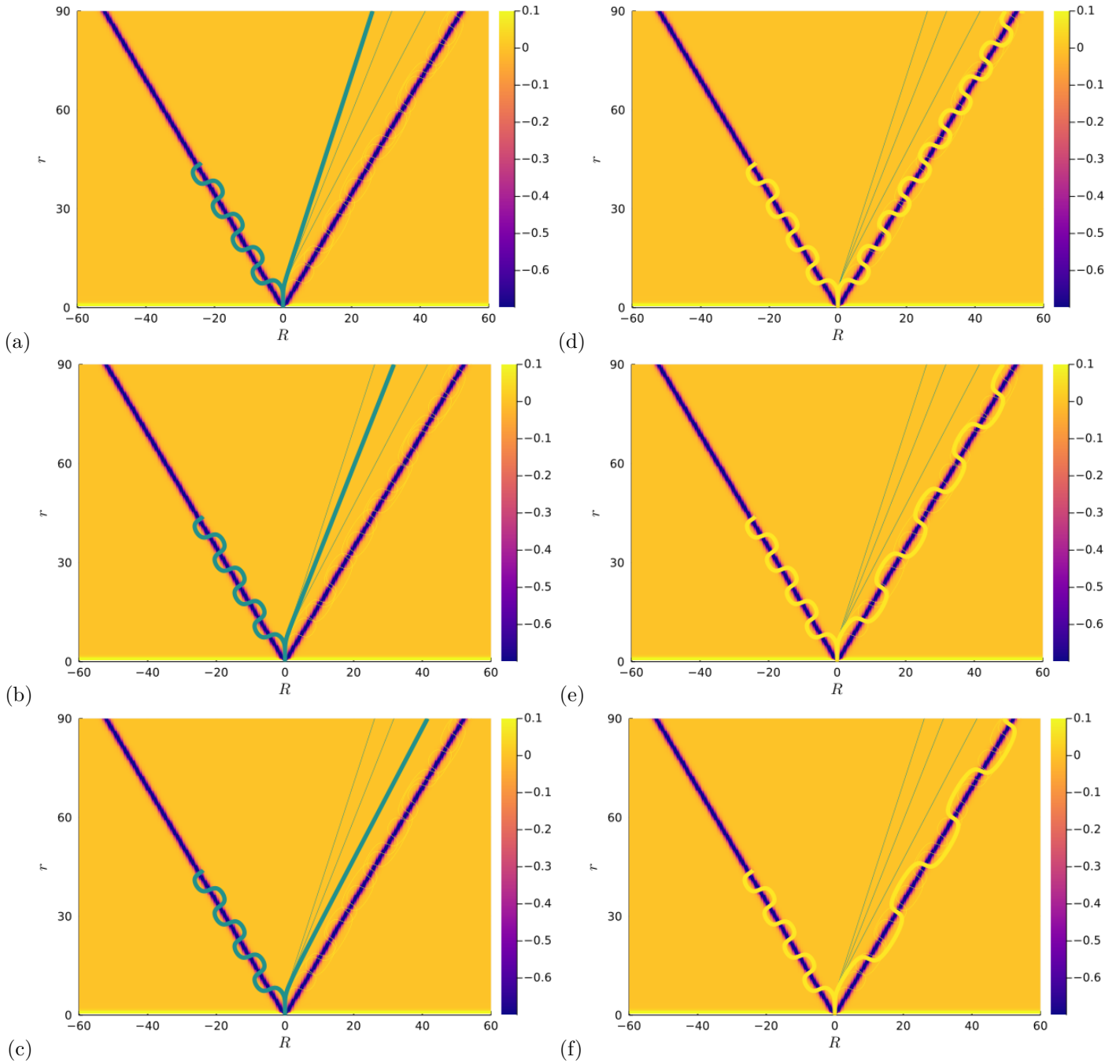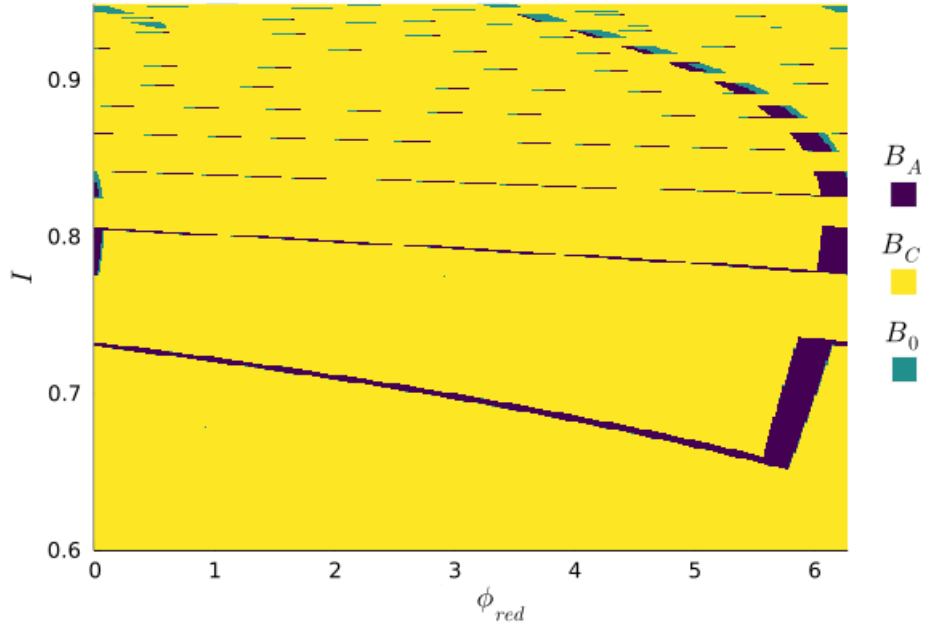
Figure 8: Trajectories close to the boundary between final asymptotic channels C and 0. $E = 0.01$, $D = 0.9$. The trajectories highlighted on the left panels end in the channel 0 and the trajectories highlighted on the right panels end in the channel C. The trajectories highlighted on lower panels are close to the boundary between channel C and 0.

Figure 9: The ϕ_{red}–I plane for fixed $E = 0.01$ in the set of initial conditions in channel A. Each pixel in this plane is coloured according to the channel in which the corresponding scattering trajectory ends in the far future. Yellow means basin B_C, cyan means basin B_A and dark blue means basin B_0.
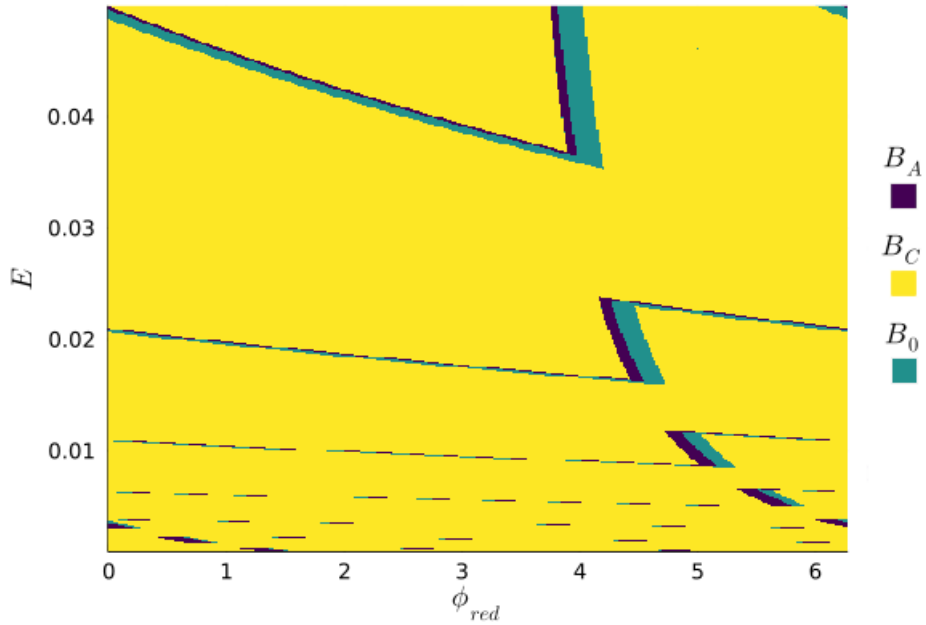

Figure 10: The ϕ_{red}–E plane for fixed $I = 0.91$ in the set of initial conditions in channel A. Each pixel in this plane is coloured according to the channel in which the corresponding scattering trajectory ends in the far future. Yellow means basin B_C, cyan means basin B_A and dark blue means basin B_0.

4 Conclusions

We have illustrated our view of the sequential decay with the help of a minimalistic model system. And now the reader may ask what are the important properties of a model system in order to be able to show the phenomenon of sequential decay. Essential is the presence of at least three particles in order to have two fragment and three fragment arrangements. And accordingly, we have basin boundaries between two fragment and three fragment final asymptotic channels. In such a setting sequential decay occurs for initial conditions inside of the basin of a three fragment channel but very close to its boundary with two fragment channels as explained in more detail at the end of section 3.

In the model system the basin boundaries for energies above the threshold of the three fragment channel are smooth because of the absence of topological chaos for positive total energy. For more complicated potentials there exist chaotic invariant sets in the phase space also for positive energies (above the three fragment threshold) which may lead to fractal basins and fractal basin boundaries. Then under a change of the total energy or some other system parameter we may have such fascinating events as basin crises and basin boundary metamorphoses. The interested reader can find detailed discussions of these events in the references [29, 30, 31, 32, 33] and also in chapter 5 of [23]. Such complicated boundaries cause additional technical difficulties of our picture of sequential decay but do not cause any changes in the basic view.

In view of our original motivation stemming from quantum systems, a comment on tunnelling is necessary. The originally mentioned decay chains as far as alpha decay and to a lesser degree other charged particle decays are concerned, are dominated by the Coulomb barrier which allows extremely long decay times. Indeed for typical reactions including cases of neutron emission in very detailed calculations, no direct three-fragment effects will be necessary to reproduce the experiments up to energies where the distorted wave Born approximations explain the phenomena. On the other hand for the molecular case, semi-classical approximations combined with the potentials obtained from Born-Oppenheimer microscopic calculations work quite well and in this case orbits near basin boundaries may well play a role not yet appreciated.

The famous picture of a wooden billiard with many balls used by Niels Bohr, is often used to show that one ball entering can well give long living excited states in classical mechanics with sequential decay in classical mechanics. This combined with Coulomb barrier effects largely explains the dominance of sequential decay in low energy scattering, at least in nuclear physics except for the smallest nuclei.

But as we mentioned already, in the three nucleon system this effect is not dominant, and Fadeev equations have to be used for a more complete understanding. Alt-Grassberger-Sandhas equations [34, 35] have been applied to few nucleon systems, but even with small nucleon numbers the deviations from sequential decays vanish quite fast, as long as energies are small.

5 Acknowledgments

References

[1] V. I. Goldansky. On neutron-deficient isotopes of light nuclei and the phenomena of proton and two-proton radioactivity. Nuclear Physics, **19**, 482 (1960). `https://doi.org/10.1016/0029-5582(60)90258-3`

[2] A. Nitzan, J. Jortner, and B. J. Berne . Interference effects in sequential decay. Molecular Physics, **26**, 281 (1973). `https://doi.org/10.1080/00268977300101631`

[3] L. R. Hafstad, and E. Teller. The alpha-particle model of the nucleus. Physical Review, **54**, 681 (1938). `https://doi.org/10.1103/PhysRev.54.681`

[4] J. A. Wheeler,. The Alpha-particle model and the properties of the nucleus Be 8. Physical Review, **59**, 27 (1941). `https://doi.org/10.1103/PhysRev.59.27`

[5] R. M. Mendez-Moreno, M. Moreno, and T. H. Seligman. Alpha particle model calculations for 12C and 16O. Nuclear Physics A, **221**, 381 (1974). `https://doi.org/10.1016/0375-9474(74)90325-X`

[6] L. Qing-Run, and Z. Jin-Li. Proton-carbon elastic scattering in the intermediate energy range based on the alpha-particle model. Journal of Physics G: Nuclear and Particle Physics, **17**, 663 (1991). `https://doi.org/10.1088/0954-3899/17/5/013`

[7] M. Freer, and H. O. U. Fynbo. The Hoyle state in 12C. Progress in Particle and Nuclear Physics, **78**, 1 (2014). `https://doi.org/10.1016/j.ppnp.2014.06.001`

[8] S. Ishikawa, S. Decay and structure of the Hoyle state. Phys. Rev. C, **90**, 061604, (2014). `https://doi.org/10.1016/j.ppnp.2014.06.001`

[9] D. Dell'Aquila, I. Lombardo, G. Verde, M. Vigilante, L. Acosta, C. Agodi, ... and A. Tumino. High-Precision Probe of the Fully Sequential Decay Width of the Hoyle State in C 12. Physical Review Letters, **119**, 132501, (2017). `https://doi.org/10.1103/PhysRevLett.119.132501`

[10] J. I. Rawlinson. An alpha particle model for Carbon-12. Nuclear Physics A, 975, 122-135 (2018). `https://doi.org/10.1016/j.nuclphysa.2018.04.011`

[11] G. Cardella, A. Bonasera, N. S. Martorana, L. Acosta, E. De Filippo, E. Geraci, ... and M. Trimarchi. Search for rare 3-α decays in the region of the Hoyle state of 12C. Nuclear Physics A, **1020**, 122395 (2022). `https://doi.org/10.1016/j.nuclphysa.2022.122395`

[12] F. M. Marqués et al. Three-body correlations in Borromean halo nuclei. Physical Review C, **64**, 061301 (2021). `https://doi.org/10.1103/PhysRevC.64.061301`

[13] S. Bagchi, R. Kanungo, Y. K. Tanaka, H. Geissel, P. Doornenbal, W. Horiuchi, ... and K. Yoshida. Two-Neutron Halo is Unveiled. Physiscal Review Letters, **124**, 222504 (2020). `https://doi.org/10.1103/PhysRevLett.124.222504`

[14] C. Maul, and K. H. Gericke. Photo induced three body decay. International Reviews in Physical Chemistry, **16**, 1-79 (1997). `https://doi.org/10.1080/014423597230307`

[15] C. Wu, C. Wu, D. Song, H. Su, Y. Yang, Z. Wu, ... and Q. Gong. Nonsequential and sequential fragmentation of CO 2 3+ in intense laser fields. Physical Review Letters, **110**, 103601 (2013). `https://doi.org/10.1103/PhysRevLett.110.103601`

[16] F. Gonzalez Montoya and S. Wiggins. Revealing roaming on the double Morse potential energy surface with Lagrangian descriptors. Journal of Physics A: Math. Theor. **53** 235702 (2020). `J.Phys.A:Math.Theor.53235702`

[17] F. Gonzalez Montoya and S. Wiggins. Phase space structure and escape time dynamics in a Van der Waals model for exothermic reactions. Physical Review E **102**, 062203 (2020). `https://doi.org/10.1103/PhysRevE.102.062203`

[18] E. E. Zotos, C. Jung and T. Saeed. The basin boundary of the breakup channel in chaotic rearrangement scattering. Nonlinear Dynamics. **104**, 705 (2021). `https://doi.org/10.1007/s11071-021-06240-6`

[19] F. Calogero. Integrable dynamical systems and related mathematical results. Nonlinear Phenomena, Proceedings of the CIFMO School and Workshop held at Oaxtepec, Lecture Notes in Physics **189**, Springer (1983). `https://doi.org/10.1007/3-540-12730-5_3`

[20] C. Jung, T. H. Seligman. Integrability of the S-matrix versus integrability of the Hamiltonian. Physics Reports **287**, 77 (1997). `https://doi.org/10.1016/S0370-1573(96)00038-5`

[21] Jorge Perez, Luis Benet, Marcelo Forets, Christopher Rackauckas, Blas Kolic, vram0gh, Elliot Saba, Julia Tag-Bot, LuEdRaMo, and agerlach (2023). PerezHz/TaylorIntegration.jl: (v0.11.0). Zenodo. `https://doi.org/10.5281/zenodo.7619071`

[22] T. Tel. The joy of transient chaos. Chaos. **25**, 97619 (2015). `https://doi.org/10.1063/1.4917287`

[23] Y-C. Lai and T. Tel, Transient Chaos, Springer (2011). `https://doi.org/10.1007/978-1-4419-6987-3`

[24] J. M. Seoane and M. A. F. Sanjuan. New developments in classical chaotic scattering. Reports on Progress in Physics **76**, 016001 (2013). `https://doi.org/10.1088/0034-4885/76/1/016001`

[25] F. Gonzalez Montoya, F. Borondo, C, Jung. Atom scattering off a vibrating surface: An example of chaotic scattering with three degrees of freedom. Communications on Nonlinear Sciences and Numerical Simulations. **90**, 105282 (2020). `https://doi.org/10.1016/j.cnsns.2020.105282`

[26] L. Reichl. The Transition to Chaos: Conservative Classical and Quantum Systems, 3rd edition, Springer (2021). `https://doi.org/10.1007/978-1-4757-4352-4`

[27] M. E. Grice, B. K. Andrews, and W. J. Chesnavich. A threshold study of the classical dynamics of collision-induced dissociation in collinear H+H2. The Journal of Chemical Physics. **87**, 959 (1987) `https://doi.org/10.1063/1.453251`

[28] J. A. Kaye and A. Kuppermann. Collinear quasiclassical trajectory study of collision-induced dissociation on a model potential energy surface. The Journal of Chemical Physics. **84**, 1463-1476 (1986) `https://doi.org/10.1063/1.450491`

[29] C. Grebogi, E. Ott and J. A. Yorke. Fractal basin boundaries, long-lived chaotic transients, and unstable-unstable pair bifurcation. Physical Review Letters **50**, 935 (1983). `https://doi.org/10.1103/PhysRevLett.50.935`

[30] J. Aguirre, J. C. Vallejo and M. A. F. Sanjuan. Wada basins and chaotic invariant sets in the Henon-Heiles system. Physical Review E **64**, 66208 (2001) `https://doi.org/10.1103/PhysRevE.64.066208`

[31] C. Grebogi, E. Ott and J. A. Yorke. Basin boundary metamorphoses: changes in accessible boundary orbits. Physica D **24**, 243 (1987) `https://doi.org/10.1016/0167-2789(87)90078-9`

[32] K. T. Alligood, L. T. L. Lali and J. A. Jorke. Metamorphoses: sudden jumps in basin boundaries. Communications in Mathematical Physics. **141**, 1 (1991) `https://doi.org/10.1016/0167-2789(87)90078-9`

[33] B. S. Park, C. Grebogi and Y. C. Lai. Abrupt dimension changes at basin boundary metamorphoses. International Journal of Bifurcation and Chaos. **02**, 533 (1992) `https://doi.org/10.1142/S0218127492000689`

[34] E. O. Alt, P. Grassberger, W. Sandhas. Reduction of the three-particle collision problem to multi-channel two-particle Lippmann-Schwinger equations. Nuclear Physics B. **2**, 2 (1967) `https://doi.org/10.1016/0550-3213(67)90016-8`

[35] E. O. Alt and P. Grassberger and W. Sandhas. Derivation of the DWBA in an exact three-particle theory. Nuclear Physics A. **139**, 1 (1969). `https://doi.org/10.1016/0375-9474(69)90271-1`